Measurement of evaporation under controlled boundary conditions

G. Gärtner, J. Grunewald & R. Plagge
Dresden University of Technology, Institute of Building Climatology, Dresden, Germany

ABSTRACT: This paper presents a new laboratory measurement setup for determination of the evaporation rate of material samples under controlled natural and forced convective air flow boundary conditions. Automatic measurements of the surface temperature and vapour flux at air temperatures and different adjusted air humidities are conducted by using wind channels placed in a climatic chamber. In addition, a new functional approach is proposed to account for the free stream air velocity and surface structure (roughness) dependency of the heat and mass surface transfer coefficients. The parameters of the functional approaches are determined by the measurements and results of six different materials are presented and analysed.

1 INTRODUCTION

A better understanding of the hygrothermal boundary conditions and of the microclimate around buildings is necessary to avoid structural and visual damage to building surfaces. For example, it is known that the growth of micro organisms as fungi or algae (Sedlbauer, 2001) depends on the microclimate at the wall surfaces. Also the durability of building surface materials (e.g. brick veneer, cladding or rendering) is affected by hygrothermal stresses due to frequency and amplitude of surface moisture content and temperature changes.

The authors believe that the term “microclimate around buildings” and its influencing parameters have not yet been satisfactorily defined. In the boundary layer theory we can find boundary layers of different thickness for heat and mass transfer but this approach does not seem very suitable to define the microclimate. On the other hand, it is most likely that the surface structure will influence the microclimate. Therefore, the authors introduce a microclimate layer which

a) is a mixed material-air zone (see Figure 1);
b) thickness is in the order of the material’s surface roughness R.

The surface material is given by its hygrothermal properties: thermal conductivity, specific heat capacity, water uptake coefficient, vapour diffusion resistance factor, porosity, ect. The conditions in the ambient air are described by air temperature, relative humidity and u_∞, the free stream air velocity. The heat and moisture exchange coefficients, α and β, stand for the transfer effects taking place in the boundary layer. In calculations, the exchange coefficients are usually treated as constants. There are also publications on determination of these coefficients as function of the air velocity (Mortensen et al. 2005, Talev et al. 2006).

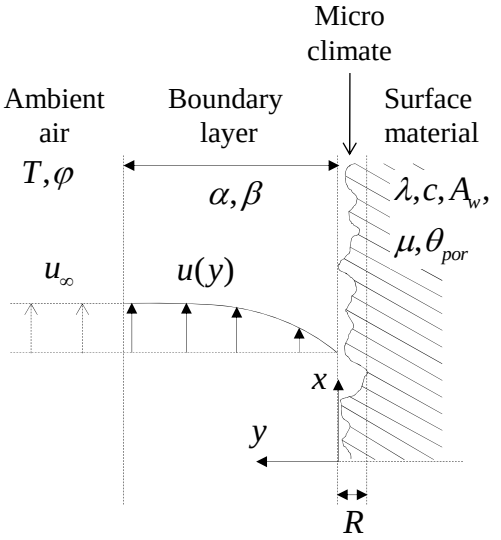

Figure 1. Definition of the microclimate layer at the wall surface and its influencing factors

Even though the microclimate is considered being dependent on all parameters depicted in Figure 1, the authors consider the exchange coefficients as the most influencing ones. The exchange coefficients are assumed to be a function of free stream air velocity and surface roughness according to equations (1) and (2).

$$\alpha = \alpha(u_\infty, R) \quad (1)$$

$$\beta = \beta(u_\infty, R) \quad (2)$$

The principal shape of the free stream air velocity dependency function in (1) and (2) is derived from the general boundary layer theory. Then a functional approach is selected to include the surface roughness as additional parameter. In the chapter “evaporation experiments” the experiments are described which have been conducted to obtain measurement results that allow determination of the function parameters by help of numerical simulation.

2 TRANSFER COEFFICIENTS MODELLING

The aim of this section is to derive a reasonable functional approach for the heat and vapour exchange coefficients (1) and (2) based on the boundary layer theory. The derivation starts with more generally defined surface transfer coefficients. The surface transfer coefficients are converted to exchange coefficients at the end of this subsection. The fundamentals of the boundary layer theory can be found in literature (Jischa 1982, Incropera et al. 2007). As far as needed, a brief summary of the theory is presented here.

Assuming steady, incompressible, laminar 2D flow with constant fluid properties and negligible viscous dissipation, the boundary layer equations can be written as balance equations for the convective mass, momentum, heat, and species transfer of a fluid phase (3) - (6).

$$\frac{\partial u}{\partial x}+\frac{\partial v}{\partial y}=0 \qquad \text{Continuity} \qquad (3)$$

$$u\frac{\partial u}{\partial x}+v\frac{\partial u}{\partial y}=\upsilon\frac{\partial^2 u}{\partial y^2} \qquad \text{Momentum} \qquad (4)$$

$$u\frac{\partial T}{\partial x}+v\frac{\partial T}{\partial y}=a\frac{\partial^2 T}{\partial y^2} \qquad \text{Energy} \qquad (5)$$

$$u\frac{\partial c}{\partial x}+v\frac{\partial c}{\partial y}=D\frac{\partial^2 c}{\partial y^2} \qquad \text{Species} \qquad (6)$$

In the above equations x, y are the spatial coordinates and u, v are the velocities. The temperature and the mass concentration are denoted by T and c, and the thermal diffusivity and species diffusivity are given by a and D, respectively.

A solution of the boundary layer equations for a flat plate in parallel flow is based on the method of Blasius, 1908. This method uses the similarity of the velocity profiles in the boundary layer stream to transform the coordinates such that an ordinary system of differential equations can be derived. The solution is simplified by the fact that conditions in the velocity boundary layer are assumed to be independent of temperature and species concentration.

New similarity variables for transformation of the coordinates x, y and velocities u, v are introduced considering the fact that the boundary layer thickness varies proportionally to square root of the distance measured from the leading edge at $L=0$ (Figure 2). The continuity equation (3) is satisfied and eliminated. Introducing the dimensionless temperature (9) and dimensionless mass concentration (10) yields a set of ordinary, non-linear differential equations of 2nd and 3rd order as (11) - (13).

$$\eta=\sqrt{\frac{u_\infty}{\upsilon}}\frac{y}{\sqrt{x}} \qquad \text{Transformation of coordinates} \qquad (7)$$

$$\frac{df}{d\eta}=f'=\frac{u(\eta)}{u_\infty} \qquad \text{Transformation of velocities} \qquad (8)$$

$$T^*\equiv\left[\left(T-T_S\right)/\left(T_\infty-T_S\right)\right] \qquad (9)$$

$$c^*\equiv\left[\left(c-c_S\right)/\left(c_\infty-c_S\right)\right] \qquad (10)$$

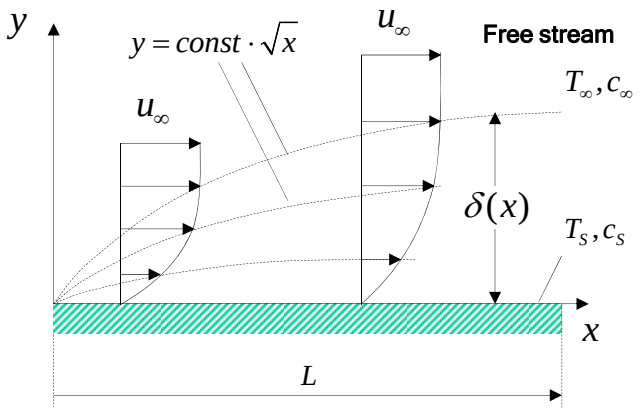

Figure 2. Similarity solution of boundary layer equations by coordinate and velocity transformation

$$\frac{d^3 f}{d\eta^3}+\frac{1}{2}f\cdot\frac{d^2 f}{d\eta^2}=0 \qquad \text{Momentum} \qquad (11)$$

$$\frac{d^2 T^*}{d\eta^2}+\frac{Pr}{2}f\cdot\frac{dT^*}{d\eta}=0 \qquad \text{Energy} \qquad (12)$$

$$\frac{d^2 c^*}{d\eta^2}+\frac{Sc}{2}f\cdot\frac{dc^*}{d\eta}=0 \qquad \text{Species} \qquad (13)$$

The dimensionless numbers in the energy and species equations are the Prandtl number Pr (ratio of the momentum and thermal diffusivities) and the Schmidt number Sc (ratio of the momentum and mass diffusivities). Both numbers are function of the fluid properties.

$$Pr=\frac{\nu}{a} \qquad \text{Prandtl number} \qquad (12)$$

$$Sc=\frac{\nu}{D} \qquad \text{Schmidt number} \qquad (13)$$

The momentum equation (11) can be numerically integrated. Its solution is given in Table 1 and the

curve in Figure 3. The gradient of the velocity profile at the surface of the plate can be obtained from the table: $f''(\eta = 0) = 0.332$.

Table 1. Numerical values of the solution of the transformed momentum equation (11). The values of first and third columns are presented in Figure 3

η	f	f'	f''
0.0	0.000	0.000	**0.332**
0.4	0.027	0.133	0.331
0.8	0.106	0.265	0.327
1.2	0.238	0.394	0.317
1.6	0.420	0.517	0.297
2.0	0.650	0.630	0.267
2.4	0.922	0.729	0.228
2.8	1.231	0.812	0.184
3.2	1.569	0.876	0.139
3.6	1.930	0.923	0.098
4.0	2.306	0.956	0.064

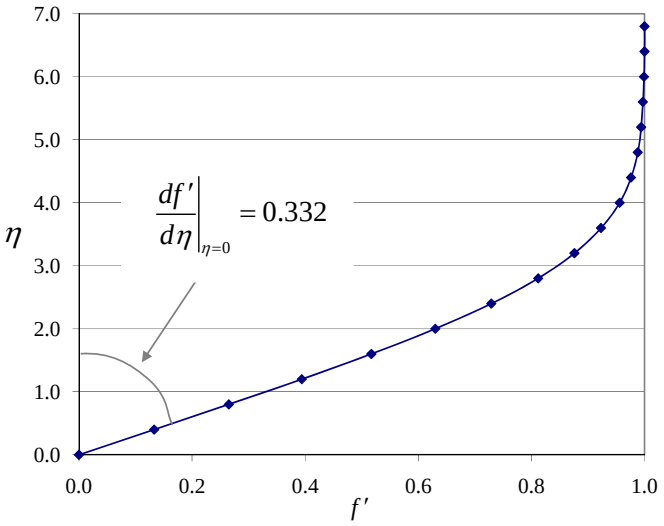

Figure 3. Graphical presentation of the numerical solution of the transformed momentum equation (11)

A similar result can be derived for the energy and species equations. Substituting f' in (11) by T^* and c^* shows the identity of (11), (12) and (13) for $Pr = Sc = 1$. In this case, the solution of the momentum equation satisfies also the energy and species equations.

For different Prandtl and Schmidt numbers the numerical solution of (12) and (13) allows establishing a dependency between the surface gradients and the Prandtl and Schmidt numbers:

$$\left.\frac{dT^*}{d\eta}\right|_{\eta=0} = 0.332 \cdot Pr^{1/3} \qquad Pr \geq 0.6 \qquad (14)$$

$$\left.\frac{dc^*}{d\eta}\right|_{\eta=0} = 0.332 \cdot Sc^{1/3} \qquad Sc \geq 0.6 \qquad (15)$$

The local heat and mass transfer coefficients, h_x and $h_{m,x}$, are defined through the energy and species flux, j_x^Q and j_x^m, and the respective temperature and concentration differences over heat and mass boundary layer thicknesses, δ_T and δ_c. The surface flux can also be expressed by the temperature and concentration gradients at the surface ($y = 0$). It should be noticed that the flux, the gradients and the transfer coefficients are function of the downstream location indicated by the subscript x.

$$j_x^Q = h_x \cdot (T_S - T_\infty) = -\lambda \left.\frac{\partial T}{\partial y}\right|_{y=0,x} \qquad (16)$$

$$j_x^m = h_{m,x} \cdot (c_S - c_\infty) = -D \left.\frac{\partial c}{\partial y}\right|_{y=0,x} \qquad (17)$$

Equations (16) and (17) are rearranged in order to derive explicit expressions for the transfer coefficients. Substituting the gradients by

$$\left.\frac{\partial T}{\partial y}\right|_{y=0,x} = -\frac{T_S - T_\infty}{x}\sqrt{\frac{u_\infty x}{\nu}} \left.\frac{\partial T^*}{\partial \eta}\right|_{\eta=0}$$

$$\left.\frac{\partial c}{\partial y}\right|_{y=0,x} = -\frac{c_S - c_\infty}{x}\sqrt{\frac{u_\infty x}{\nu}} \left.\frac{\partial c^*}{\partial \eta}\right|_{\eta=0}$$

yields

$$h_x = -\frac{\lambda}{x}\sqrt{\frac{u_\infty x}{\nu}} \left.\frac{\partial T^*}{\partial \eta}\right|_{\eta=0} \qquad (18)$$

$$h_{m,x} = -\frac{D}{x}\sqrt{\frac{u_\infty x}{\nu}} \left.\frac{\partial c^*}{\partial \eta}\right|_{\eta=0}. \qquad (19)$$

The term under the square roots in (18) and (19) is the local Reynolds number Re_x which is a function of the free stream velocity u_∞. With (14) and (15) we can now establish a relation between the surface transfer coefficients and the free stream velocity.

$$h_x = \frac{\lambda}{x} \cdot Re_x^{1/2} \cdot 0.332 \cdot Pr^{1/3} \qquad (20)$$

$$h_{m,x} = \frac{D}{x} \cdot Re_x^{1/2} \cdot 0.332 \cdot Sc^{1/3} \qquad (21)$$

For practical calculations average transfer coefficients over a certain characteristic length L are of interest.

$$h = \frac{1}{x}\int_0^L h_x dx = \frac{\lambda}{L} \cdot Re^{1/2} \cdot 0.664 \cdot Pr^{1/3} \qquad (20)$$

$$h_m = \frac{1}{x}\int_0^L h_{m,x} dx = \frac{D}{L} \cdot Re^{1/2} \cdot 0.664 \cdot Sc^{1/3} \qquad (21)$$

A generalized approach introduces the constants C and m to account for different geometry, orientation and flow conditions (laminar, turbulent). The input parameters to (22) and (23) are listed below.

$$h = \frac{\lambda}{L} \cdot C \cdot Re^m \cdot Pr^{1/3} \tag{22}$$

$$h_m = \frac{D}{L} \cdot C \cdot Re^m \cdot Sc^{1/3} \tag{23}$$

Input parameters:

- Thermo-physical properties of the fluid (air):
  - Thermal conductivity λ = 0.0263 W/mK
  - Specific heat capacity c_p = 1000 J/kgK
  - Density ρ = 1.25 kg/m^3
  - Viscosity ν = 1.55E-05 m^2/s
  - Reference pressure p_{ref} = 101325 Pa
  - Reference temperature T = 20°C
- Thermo-physical properties of species (water vapour):
  - Specific gas constant R_v = 462 J/kgK
- Functional parameters of (22) and (23):
  - Characteristic length[1] L = 0.1, 0.5, 1, 5 m
  - Slope constant[2] C = 0.664, 0.193, 0.027
  - Exponent[2] m = 0.500, 0.618, 0.805

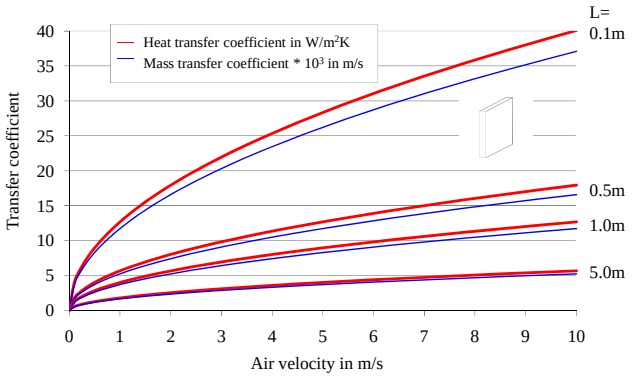

Figure 4. Heat and mass transfer coefficients of a flat plate.

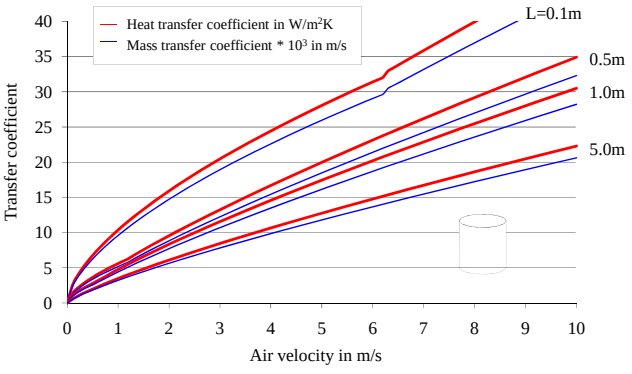

Figure 5. Heat and mass transfer coefficients of a cylinder.

The transfer coefficients for a flat plate and for a cylindrical shape are depicted in Figures 4 and 5.

[1] Four values of characteristic length are used as a parameter.

[2] Three values are used: 1. for flat plate, 2. for cylinder with Re<40000 (laminar) and 3. for cylinder with Re>=40000 (turbulent)

The gradients of temperature and mass concentration at the surface of the plate vanish at zero air velocity. Consequently, the transfer coefficients become zero at zero air velocity. In reality, even for zero air velocity, there should be diffusive transport of heat and mass. For lower air velocity the diffusive transport dominates, for higher air velocity the convective transport prevails. Therefore, the functional approaches for transfer coefficients should be corrected for diffusive processes at zero air velocity by introducing offset values. The heat and vapour exchange coefficients are given by (24) and (25), in which α_0 and β_0 are the offset values. The slope constants α_{ref} and β_{ref} are defined at zero offset and reference velocity u_{ref}.

$$h = \alpha(u_\infty, R) = \alpha_0 + \alpha_{ref}(R) \cdot \left(\frac{u_\infty}{u_{ref}} \right)^n \tag{24}$$

$$\frac{h_m}{R_v T} = \beta(u_\infty, R) = \beta_0 + \beta_{ref}(R) \cdot \left(\frac{u_\infty}{u_{ref}} \right)^n \tag{25}$$

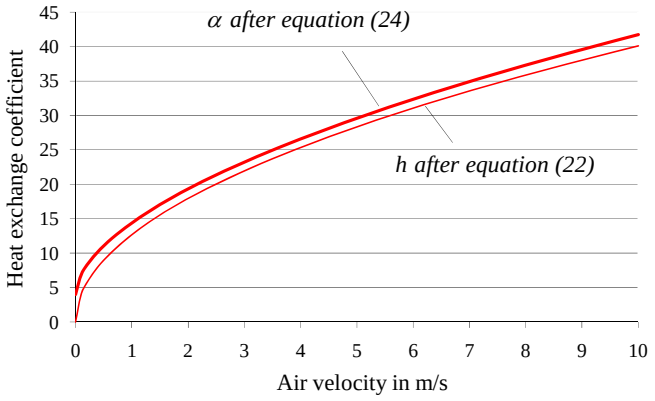

Figure 6. Comparison of heat exchange coefficient (with α_0=4 W/m^{2}K, α_{ref}=27 W/m^{2}K, u_{ref}=5.5 m/s, n=0.56) and heat transfer coefficient (for a flat plate with L=20cm)

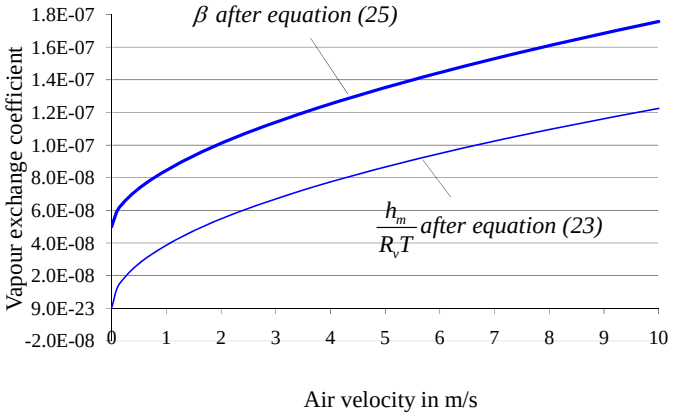

Figure 7. Comparison of vapour exchange coefficient (with β_0=5e-8 kg/m^{2}Pas, β_{ref}=9e-8 kg/m^{2}Pas, u_{ref}=5.5 m/s, n=0.56) and mass transfer coefficient (for a flat plate with L=50cm)

It should be noticed that in (25) the water vapour exchange coefficient β is related to partial pressure

difference while the mass transfer coefficient h_m is related to the concentration difference. Both coefficients can be easily converted to each other by using the ideal gas equation for water vapour.

The exponent n is used to fit the curvature of both, the heat and vapour exchange coefficients. The exponent is given by the principal shape of the curves from the boundary layer theory. In (24) and (25) the reference values, α_{ref} and β_{ref}, are defined as function of R to take the surface roughness into consideration. The offset values are determined by experiments at zero air velocity while the reference values are measured at reference air velocity.

3 EVAPORATION EXPERIMENT SETUPS

Two types of experiments are designed to gather evaporation data under controlled laboratory boundary conditions. Natural (almost still air) and forced air flow can be realised. The experimental installations were placed in a climatic chamber where temperature and relative humidity can be properly controlled. Initially saturated samples are dried by evaporation. The evaporation rates are measured by automatic weighting of the samples.

3.1 *Natural air flow experiment (*$u_\infty = 0$ m/s*)*

The natural air flow experimental setup (Figure 8) for obtaining the offset value β_0 is intended to realize zero air flow conditions. Buoyancy effects cannot completely be excluded but the conditions are kept as constant as possible. The container has been designed to measure 6 samples at the same time.

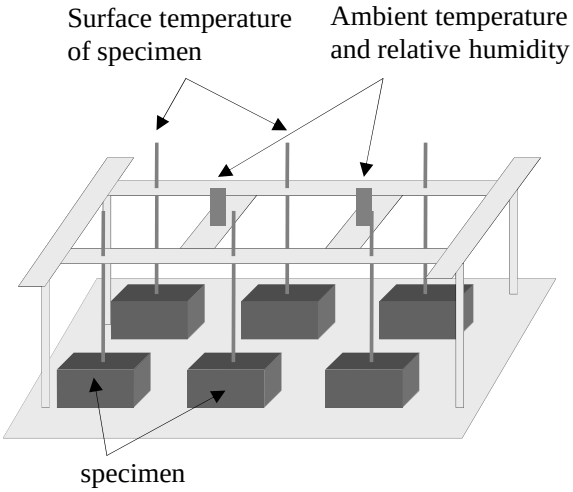

Figure 8. Apparatus and sensor installations for automatic measurement of evaporation rate under natural air flow conditions

The setup is equipped with NTC sensors (negative temperature coefficient) for measuring the surface temperature as well as the temperature and relative humidity in the surrounding area. The sensors are connected to a data acquisition system where the recorder was set to a 10 minute collection rate. The total weight of the samples was measured manually two times a day.

3.2 *Forced convection experiment (*$u_\infty = 5.5$ m/s*)*

A second experimental setup with three specially designed wind channels has been built to gather data under forced convection conditions. A schematic drawing of the experimental setup is given in Figures 9.

The wind channels are equipped with infrared sensors for measuring the surface temperature of the sample material. Additionally, the air temperature and relative humidity along the rectangular cross section are measured by an NTC temperature sensor. The total weight of the sample is measured by a balance. All sensors and the balance are connected to a data acquisition system where the recorder was set to a 10 minute collection rate.

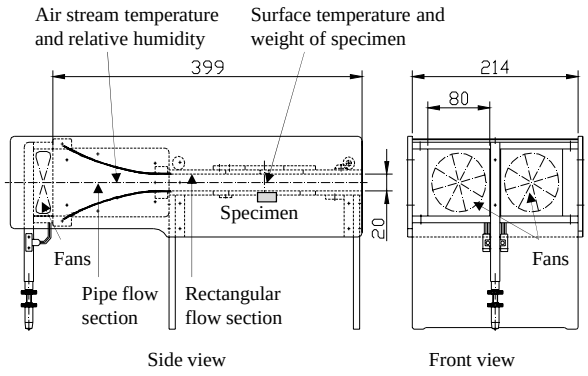

Figure 9. Experimental setup for automatic measurement of evaporation rate under forced convection conditions

In each wind channel the specimen of 50 mm diameter and 25 mm height are placed with their surface plane to the inside bottom plate of the wind channel. The surface ideally fits the bottom plate to avoid disturbances of the air stream by surface discontinuities.

The initial conditions are 23°C and 35, 65 or 85% relative humidity in the climate chamber. The wind velocity is adjusted for all forced convection-type measurements to $u_\infty = 5.5$ m/s with a measured tolerance of 0.5 m/s in the region of the sample surfaces.

4 EVALUATION OF MEASUREMENTS

4.1 *Measured and simulated drying curves*

The drying curves show significant differences between natural and forced air flow conditions as depicted by the dotted lines in Figure 10. The curves

are fitted by numerical simulation[3] of the specimen's drying behaviour in order to determine the above defined parameters of the heat and vapour exchange coefficients.

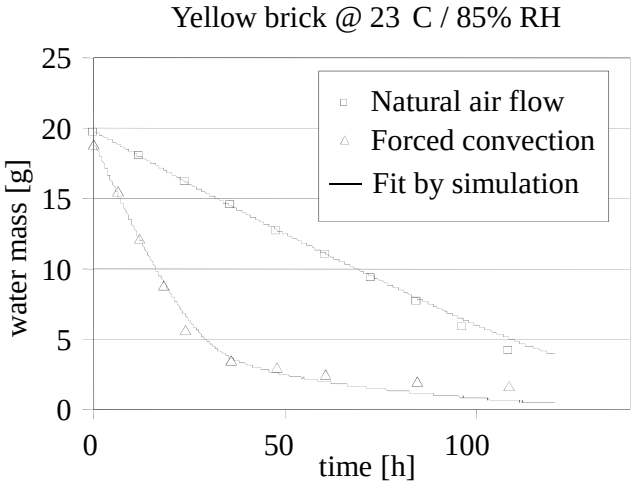

Figure 10. Measured and simulated drying curves of yellow brick under natural and forced convection air flow conditions

Since the air velocity can be assumed being constant for both, natural and forced air flow conditions, the two types of experiments can be fitted by constant exchange coefficients, respectively: $\beta_0 = \text{const}$ and $\beta(u_\infty, R) = const$. Important is the correct modelling of the evaporation cooling effect. The surface temperature drop due to evaporation cooling can be up to 5 K during the first intensive drying phase and the drying surface temperature is not uniformly distributed. This means the drying experiments are 3D or 2D rotation-symmetric simulation problems.

The simulation software uses a set of basic parameters and material functions to characterise the transport and storage properties of porous materials:

- moisture retention curve,
- thermal conductivity,
- water vapour diffusivity and
- liquid water conductivity.

The material functions of more than 120 different materials have been measured at the Building Physical Laboratory of the Institute of Building Climatology[4]. Six materials were selected for demonstration of the evaluation procedure:

- Yellow brick,
- Ceramic brick,
- Lime sandstone,
- Sandstone,
- Autoclaved aerated concrete
- Calcium silicate thermal insulation.

[3] The hygrothermal simulation software Delphin6 was used being available under *www.bauklimatik-dresden.de*

[4] See laboratory web page under *www.bauklimatik.de*

The first series of measurements and simulations were carried out to investigate the influence of the air velocity on the vapour exchange coefficient. Since the surface roughness is expected to affect the slope parameter $\beta_{ref}(R)$, a second and a third series of measurements and simulations were conducted.

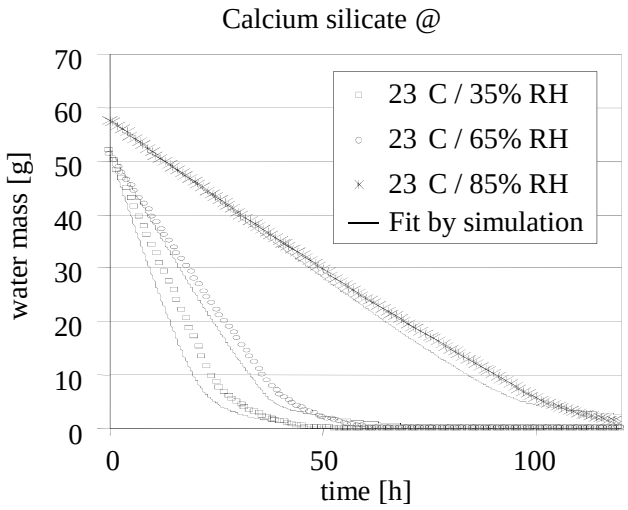

Figure 11. Measured and simulated drying curves of calcium silicate (smooth material) at different relative humidity under forced convection air flow conditions

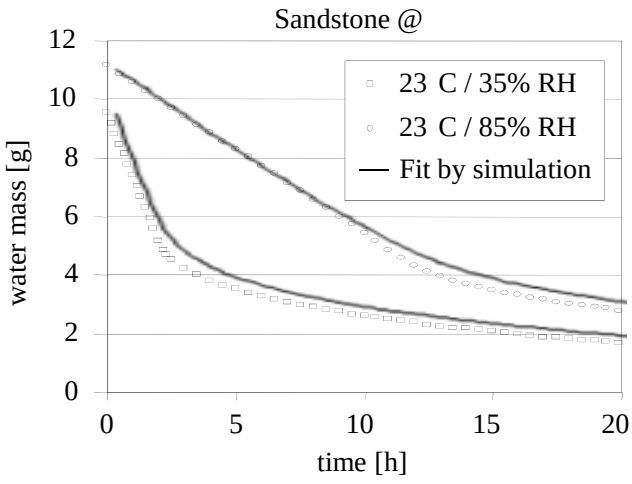

Figure 12. Measured and simulated drying curves of sandstone (rough material) under forced convection air flow conditions

A material with a relatively smooth surface and a material with a relatively rough surface under varying relative humidity in the forced convection air flow were selected for graphical presentation. While the surface roughness of calcium silicate is estimated being smaller than 10 µm the surface roughness of sandstone is about 500 µm. More precise measurements of the surface roughness are planned. The measured and fitted drying curves of both materials are depicted in Figures 11 and 12.

4.2 *Summary of fitted parameters*

The parameter fitting results of the simulations carried out to approximate the measured drying curves

are listed in Table 2 for the six materials under investigation. For each material the two types of experiments under natural and forced convection air flow conditions have been conducted. For the zero air flow conditions the offset parameter β_0 was used to fit the experimental curves, while $\beta(u_\infty, R)$ was used to fit the curves under forced convection air flow conditions.

Table 2. Results of the parameters fitting simulations for 6 building materials of different surface roughness under natural and forced convection air flow conditions

	u_∞ = 0 m/s	u_∞ = 5.5 m/s	
Material	β_0	$\beta(u_\infty, R)$	$\beta_{ref}(R)$
	kg/(m^{2}Pa s)	kg/(m^{2}Pa s)	kg/(m^{2}Pa s)
Yellow brick	3.30E-08	1.35E-07	1.02E-07
Ceramic brick	4.90E-08	1.50E-07	1.01E-07
Lime sandstone	4.20E-08	1.80E-07	1.38E-07
Sandstone	6.80E-08	1.80E-07	1.12E-07
Aerated concrete	2.80E-08	6.80E-08	4.00E-08
Calcium silicate	4.20E-08	1.70E-07	1.28E-07

The values reported in Table 2 allow some interesting observations and conclusions:

1. We notice that the vapour exchange coefficients become generally larger under forced convection. This is in agreement with the theoretical anticipations.
2. We can see that the β_0 values vary in a narrow range while the values of $\beta(u_\infty, R)$ appear to be more scattered.
3. The curves depicted in Figure 11 are fitted with one constant calcium silicate value for $\beta(u_\infty, R)$ while the curves depicted in Figure 12 are fitted with another constant sandstone value for $\beta(u_\infty, R)$.
4. The slope parameter $\beta_{ref}(R)$ can be calculated as function of surface roughness from measurements at two different air velocities.

5 CONCLUSIONS

The vapour exchange coefficient increases with higher air velocity. The general shape of the function follows from the boundary layer theory. It is necessary to introduce an offset value to account the for diffusion process at zero air velocity.

The vapour exchange coefficient is little dependent on the material as long as the air velocity is low. The surface roughness becomes an important factor at higher air velocity. The influence of the relative humidity can be neglected.

ACKNOWLEDGEMENTS

We are very grateful to be supported by the European Structural Fund and the Free State of Saxony by the project number: 80937456.

REFERENCES

Baehr, H. D. & Stephan, K. 2006. *Wärme- und Stoffübertragun,. Publisher Springer*. Berlin.

Incropera, F.P., Dewitt, D.P., Bergman, T.L., Lavine, A.S. 2006. *Fundamentals of heat and mass transfer. Publisher John Wiley & Sons*. Hoboken

Jacobsen, S. & Aarseth, L. 1998. *Effect of wind on drying from wet porous building materials surfaces- A simple model in steady state, Materials and Structures, Vol. 32, pp 38-44*.

Jischa, M. 1982. *Konvektiver Impuls-, Wärme- und Stoffaustausch, Vieweg & Sohn Verlagsgesellschaft mbH*, Braunschweig.

Krischer, O. & Kröll, K. 1956. *Trocknungstechnik Bd.1, Springer*, Berlin, Göttingen, Heidelberg.

Mortensen L.H., Rode C., Peuhkuri R., 2005. *Effect of airflow velocity on moisture exchange at surfaces.* Website of the IEA Annex 41 project (MOIST-ENG), http://www.kuleuven.be/bwf/projects/annex41/index.htm by Danish Technical University (DTU)

Scheffler, G. & Plagge, R. 2005. *Bestimmung des Trocknungsverhaltes von Baustoffen unter definierten Randbedingungen, Bauphysik 27, Heft 6 Ernst & Sohn*.

Scheffler G. & Plagge, R. 2009. *Ein Trocknungskoeffizient für Baustoffe, Bauphysik 31, Heft 3 Ernst & Sohn*.

Sedlbauer K. 2001 *Prediction of mould fungus formation in the surface of and inside building* components, Institut for Building Physik, Holzkirchen.

Talev G., Gustavsen A. & Næssb E. 2006. *The influence of air velocity and transport properties on the surface mass transfer coefficient in a rectangular tunnel – theory and experiment.* Website of the IEA Annex 41 project (MOIST-ENG), http://www.kuleuven.be/bwf/projects/annex41/index.htm by Norwegian University of Science and Technology (NTNU)

Zhang, J.S. & Grunewald J. 2007. *Prediction of the mold fungus formation probability on critical building components in residential dwellings, Center of Excellence*, Syracuse.